Semi-active control of independently rotating wheels in railway vehicles

T. X. Mei, H. Li, A. Zaeim & H. Y. Dai

Published online: 04 Jan 2024.

Submit your article to this journal ↗

Article views: 438

View related articles ↗

View Crossmark data ↗

🔓 OPEN ACCESS   Check for updates

Semi-active control of independently rotating wheels in railway vehicles

T. X. Mei[a], H. Li[b], A. Zaeim[a] and H. Y. Dai[c]

[a]School of Science, Engineering and Environment, University of Salford, Salford, UK; [b]School of Engineering, Manchester Metropolitan University, Manchester, UK; [c]State Key Laboratory of Rail Transit Vehicle Systems, Southwest Jiaotong University, Chengdu, People's Republic of China

ABSTRACT

This paper presents an in-depth analysis of steering and guidance problems of independently rotating wheels (IRWs) in railway vehicles and provides an engineering insight into the possibilities for passive and/or semi-active control possibilities that do not require expensive full-active systems. The theoretical development is then supported in the study by carrying out a comprehensive performance evaluation in comparison with a full active control. The study demonstrates that the independently rotating wheelset may be effectively controlled via semi-active approaches to provide the wheelsets with the necessary steering on curves and self-centring ability on a straight track with irregularities with performance comparable with full active systems.

List of symbols and parameters

C_{MR}, C_{min}	Damping coefficient of MR damper ($C_{min} = 62.5$ Ns/m)
f_{11}, f_{22}	Creep coefficient
F_{demand}	Control demand of the wheelset controller
G_1, G_2	Control gains ($G_1 = 65$ kNs/m, $G_2 = 1500$ Ns/m)
g	Gravitational constant
I	Yaw inertia of wheelset (700 kg.m^2)
J	Rotation inertia of wheels (100 kg.m^2)
L	Wheelset half gauge (0.75 m)
m	Mass of wheelset (1250 kg)
R	Track curve radius
ro	Wheel radius (0.45 m)
T_R, T_X	Control input
V	Vehicle speed (m/s)
ΔV	Relative velocity of the MR damper
y	Wheelset lateral displacement (m)
y_t	Track lateral displacement

CONTACT T X Mei ✉ t.x.mei@salford.ac.uk

θ	Track cant angle (6º)
λ	Wheel conicity (0.2)
ψ, Ψ	Wheelset yaw angle
$\Delta\omega$, $\Delta\Omega$	Relative rotational velocity between two wheels

Vehicle mass (34,460 kg)
    Bogie frame mass, without the wheelsets (3447 kg)
    Distance between two bogie centres (19.0 m)
    Distance between two wheelsets (2.5 m)
    Primary lateral stiffness (511 kN/m)
    Primary damping per wheelset (37 kNs/m)
    Secondary lateral stiffness (471 kN/m)
    Secondary damping per wheelset (12 kN/m)

1. Background

Independently rotating wheelsets are sometimes preferred in railway vehicles for applications where the presence of axles is undesirable and/or where there is a need to avoid the kinematic hunting problem of solid-axle wheelsets and the difficult trade-off between the stability and curving performance in the design of passive suspensions. However, the free movement between the two wheels causes an independently rotating wheelset to lose the natural curving and track-following ability of the solid-axle wheelset, and extra steering actions are needed if the wheels running on flanges and excessive wear are to be avoided. Passive steering mechanisms such as those used on Talgo trains may be used to provide the missing curving actions, although active solutions can offer much more effective solutions [1].

There has been a lot of interest in the study of active control strategies for independently rotating wheelsets, and it has been shown that the active control for IRWs requires a much lower level of power than that for the solid-axle wheelset [1, 2]. A number of control configurations have been proposed, including actuation to apply a yaw torque to the wheelset[3–5], independently driven wheels to apply a differential torque to the two wheels of an IRW [6–8], and directly steered wheelset[9, 10]. Steering and guidance control may be provided through equal wheel speed [4, 5] or zero lateral clearance [7,9]. Alternatively, model-based approach may be employed to design control laws with practical sensors [3].

However, full active control systems require the use of actuators that are capable of both injecting into and dissipate energy from the system and such actuators are not only expensive but also tend to be bulky in size – this can lead to considerable increase in the overall costs of railway vehicles and also difficulties in installations in space tight bogie frames. In addition, active wheelset control is safety critical and increased costs for hardware redundancies could potentially hinder or even prevent practical adoption of such technologies for commercial applications despite its clear advantages [1].

Semi-active control approaches offer a possible compromise, as variable dampers can be much lower in cost and more compact in size compared with the full active actuators. On the other hand, the control of railway wheelsets must be provided continuously for safety reasons, unlike the second suspensions for ride quality improvements [11]. Therefore, the

main research challenge is to develop semi-active control schemes that can deliver the continued steering/guidance actions within the obvious constraint of energy dissipation only, i.e. no energy injection into the system. A previous study has shown that it is possible to use controllable MR dampers for the provision of steering and guidance control [12]. This paper will, however, carry out an in-depth analysis of steering and guidance problems of independently rotating wheels and provides an engineering insight into the passive and semi-active control possibilities. A comprehensive performance evaluation will then be presented and compared with full active control to demonstrate that the independently rotating wheelset may be effectively controlled via semi-active approaches to provide the wheelsets with the necessary steering on curves and self-centring ability on a straight track with irregularities.

2. Control analysis

The linearised model of an independently rotating wheelset is used in the analysis and development of steering control strategies, as given in Equations (1)–(3) where T_X and T_R are possible control inputs in the yaw and rotational directions [3]:

$$m\ddot{y} + \frac{2f_{22}}{V}\dot{y} - 2f_{22}\psi = m\left(\frac{V^2}{R} - g\theta\right) \tag{1}$$

$$J\ddot{\psi} + \frac{2f_{11}L^2}{V}\dot{\psi} + \frac{2f_{11}\lambda L}{r_0}y + \frac{2r_0 f_{11}L}{V}\Delta\omega = \frac{2f_{11}L^2}{R} + \frac{2f_{11}\lambda L}{r_0}y_t + T_X \tag{2}$$

$$I\dot{\Delta\omega} + \frac{f_{11}r_0^2}{V}\Delta\omega + f_{11}\lambda y + \frac{r_0 f_{11}L}{V}\dot{\psi} = \frac{r_0 f_{11}L}{R} + f_{11}\lambda y_t + T_R \tag{3}$$

The corresponding state-space equation of the model is shown in Equation (4) for the purpose of control analysis.

$$\frac{d}{dt}\begin{bmatrix} \dot{y} \\ y \\ \dot{\psi} \\ \psi \\ \Delta\omega \end{bmatrix} = \begin{bmatrix} -\frac{2f_{22}}{mV} & 0 & 0 & \frac{2f_{22}}{m} & 0 \\ 1 & 0 & 0 & 0 & 0 \\ 0 & -\frac{2f_{11}\lambda L}{Jr_0} & -\frac{2f_{11}L^2}{JV} & 0 & -\frac{2r_0 f_{11}L}{VJ} \\ 0 & 0 & 1 & 0 & 0 \\ 0 & -\frac{f_{11}\lambda}{I} & -\frac{r_0 f_{11}L}{IV} & 0 & -\frac{f_{11}r_0^2}{VI} \end{bmatrix}\begin{bmatrix} \dot{y} \\ y \\ \dot{\psi} \\ \psi \\ \Delta\omega \end{bmatrix} + \begin{bmatrix} 0 & 0 \\ 0 & 0 \\ \frac{1}{J} & 0 \\ 0 & 0 \\ 0 & \frac{1}{I} \end{bmatrix}\begin{bmatrix} T_X \\ T_R \end{bmatrix}$$

$$+ \begin{bmatrix} V^2 & -g & 0 \\ 0 & 0 & 0 \\ \frac{2f_{11}L^2}{J} & 0 & \frac{2f_{11}\lambda L}{Jr_0} \\ 0 & 0 & 0 \\ \frac{r_0 f_{11}L}{I} & 0 & \frac{f_{11}\lambda}{I} \end{bmatrix}\begin{bmatrix} \frac{1}{R} \\ \theta \\ y_t \end{bmatrix} \tag{4}$$

Or

$$
\frac{d}{dt}
\begin{bmatrix} \dot{y} \\ y \\ \dot{\psi} \\ \psi \\ \Delta\omega \end{bmatrix}
=
\begin{bmatrix}
-a_{11} & 0 & 0 & a_{14} & 0 \\
1 & 0 & 0 & 0 & 0 \\
0 & -a_{32} & -a_{33} & 0 & -a_{35} \\
0 & 0 & 1 & 0 & 0 \\
0 & -a_{52} & -a_{53} & 0 & -a_{55}
\end{bmatrix}
\begin{bmatrix} \dot{y} \\ y \\ \dot{\psi} \\ \psi \\ \Delta\omega \end{bmatrix}
+
\begin{bmatrix}
0 & 0 \\
0 & 0 \\
b_{31} & 0 \\
0 & 0 \\
0 & b_{52}
\end{bmatrix}
\begin{bmatrix} T_X \\ T_R \end{bmatrix}
$$

$$
+
\begin{bmatrix}
w_{11} & w_{12} & 0 \\
0 & 0 & 0 \\
w_{31} & 0 & w_{33} \\
0 & 0 & 0 \\
w_{51} & 0 & w_{53}
\end{bmatrix}
\begin{bmatrix} \frac{1}{R} \\ \theta \\ y_t \end{bmatrix}
\tag{5}
$$

where

$$
A =
\begin{bmatrix}
-\frac{2f_{22}}{mV} & 0 & 0 & \frac{2f_{22}}{m} & 0 \\
1 & 0 & 0 & 0 & 0 \\
0 & -\frac{2f_{11}\lambda L}{Jr_0} & -\frac{2f_{11}L^2}{JV} & 0 & -\frac{2r_0 f_{11}L}{VJ} \\
0 & 0 & 1 & 0 & 0 \\
0 & -\frac{f_{11}\lambda}{I} & -\frac{r_0 f_{11}L}{IV} & 0 & -\frac{f_{11}r_0^2}{VI}
\end{bmatrix}
; B =
\begin{bmatrix}
0 & 0 \\
0 & 0 \\
\frac{1}{J} & 0 \\
0 & 0 \\
0 & \frac{1}{I}
\end{bmatrix}
;
$$

$$
W =
\begin{bmatrix}
V^2 & -g & 0 \\
0 & 0 & 0 \\
\frac{2f_{11}L^2}{J} & 0 & \frac{2f_{11}\lambda L}{Jr_0} \\
0 & 0 & 0 \\
\frac{r_0 f_{11}L}{I} & 0 & \frac{f_{11}\lambda}{I}
\end{bmatrix}
$$

Close examination of A matrix reveals that the yaw motion (in row 3) and the relative rotation motion (row 5) are dependent on each other with a common scaling factor, $Jr_0/(2LI)$, and therefore A is not full rank and there is a pole at $s = 0$. This can be readily proven using an additional matrix K as demonstrated in Equation (6)

$$
KA =
\begin{bmatrix}
1 & 0 & 0 & 0 & 0 \\
0 & 1 & 0 & 0 & 0 \\
0 & 0 & 1 & 0 & 0 \\
0 & 0 & 0 & 1 & 0 \\
0 & 0 & -1 & 0 & -\frac{Jr_0}{2LI}
\end{bmatrix}
\begin{bmatrix}
-\frac{2f_{22}}{mV} & 0 & 0 & \frac{2f_{22}}{m} & 0 \\
1 & 0 & 0 & 0 & 0 \\
0 & -\frac{2f_{11}\lambda L}{Jr_0} & -\frac{2f_{11}L^2}{JV} & 0 & -\frac{2r_0 f_{11}L}{VJ} \\
0 & 0 & 1 & 0 & 0 \\
0 & -\frac{f_{11}\lambda}{I} & -\frac{r_0 f_{11}L}{IV} & 0 & -\frac{f_{11}r_0^2}{VI}
\end{bmatrix}
$$

$$
=
\begin{bmatrix}
-\frac{2f_{22}}{mV} & 0 & 0 & \frac{2f_{22}}{m} & 0 \\
1 & 0 & 0 & 0 & 0 \\
0 & -\frac{2f_{11}\lambda L}{Jr_0} & -\frac{2f_{11}L^2}{JV} & 0 & -\frac{2r_0 f_{11}L}{VJ} \\
0 & 0 & 1 & 0 & 0 \\
0 & 0 & 0 & 0 & 0
\end{bmatrix}
\tag{6}
$$

It is clear that K is full rank, as all diagonal elements are non-zero and all elements above the diagonal are zero. It is also true that the rank of K∗A (both 5×5 in dimension) will be

T. X. MEI ET AL.

Table 1. Typical poles (eigenvalues) of independently rotating wheelset at low and high speeds.

	V = 90 km/h (25 m/s)			V = 300 km/h (83 m/s)	
Poles	Damping (%)	Frequency (rads/s)	Poles	Damping (%)	Frequency (rads/s)
−640	100	640	−189	100	189
−138	100	138	−66.6	100	66.6
0.71 ± 12.6i	−5.6	12.7	11.4 ± 31.6i	−34	33.6
0	0	0	0	0	0

the same as that of A, i.e. rank(A) = rank(K∗A). In this case, K∗A is clearly not full rank due to all elements in row 5 being 0, therefore A is not full rank.

The dependency between the yaw and the relative rotation means that the two motions are in phase and it is the root cause for the lack of steering of the independently rotating wheelsets. Factors such as gravitational stiffness can help to provide limited capability of track following, but additional steering measures will be necessary to avoid wheelsets running on flanges and excessive wear especially on tight curves. Steering control may be provided by applying a yaw torque (T_X) to the independently rotating wheelsets, or a differential torque (T_R) to the two wheels in the rotational direction. The two approaches play very similar roles because of the dependency between the two motions. This study is focused on the application of the yaw torque but will aim to study control options that may be implemented with the use of passive and/or semi-active devices.

Numerical analysis of the independently rotating wheelset reveals that, in addition to the lack of steering action due to the pole s = 0, there is also a pair of positive complex poles representing a dynamic instability as shown in Table 1. This dynamic instability has also been reported before in the literature [3, 4].

The implementation with passive and/or semi-active means requires no power injection from the control devices and two possibilities are to use the velocity feedback such as the yaw velocity and/or relative rotational velocity and then to apply a control effort in the same phase as the motions. The transfer functions between the two velocity feedback cases and the yaw torque are given in Equations (7) and (8).

$$\frac{s\Psi(s)}{T_x(s)} = \frac{s^2(s + a_{11})(s + a_{55})}{s(s^4 + T_3 s^3 + T_2 s^2 + T_1 s + T_0)} \tag{7}$$

$$\frac{\Delta\Omega(s)}{T_x(s)} = \frac{b_{31}(a_{53}s^3 + a_{11}a_{53}s^2 + a_{52}a_{14})}{s(s^4 + T_3 s^3 + T_2 s^2 + T_1 s + T_0)} \tag{8}$$
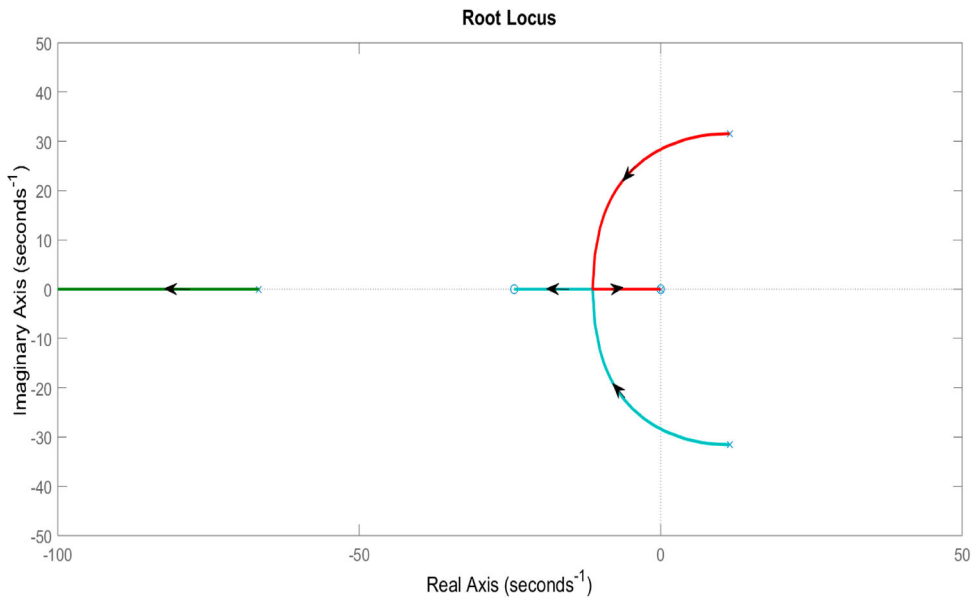
where

$$T_3 = a_{11} + a_{33} + a_{55}$$

$$T_2 = a_{11}a_{33} + a_{11}a_{55} + a_{33}a_{55} - a_{35}a_{53}$$

$$T_1 = a_{11}a_{33}a_{55} - a_{11}a_{35}a_{53}$$

$$T_0 = a_{14}a_{32}$$

The pole at s = 0 in the transfer functions again confirms the lack of track-following ability of the independently rotating wheelsets so it needs to be moved away from 0 to an appropriate negative value for the purpose of steering. Unfortunately, this cannot be
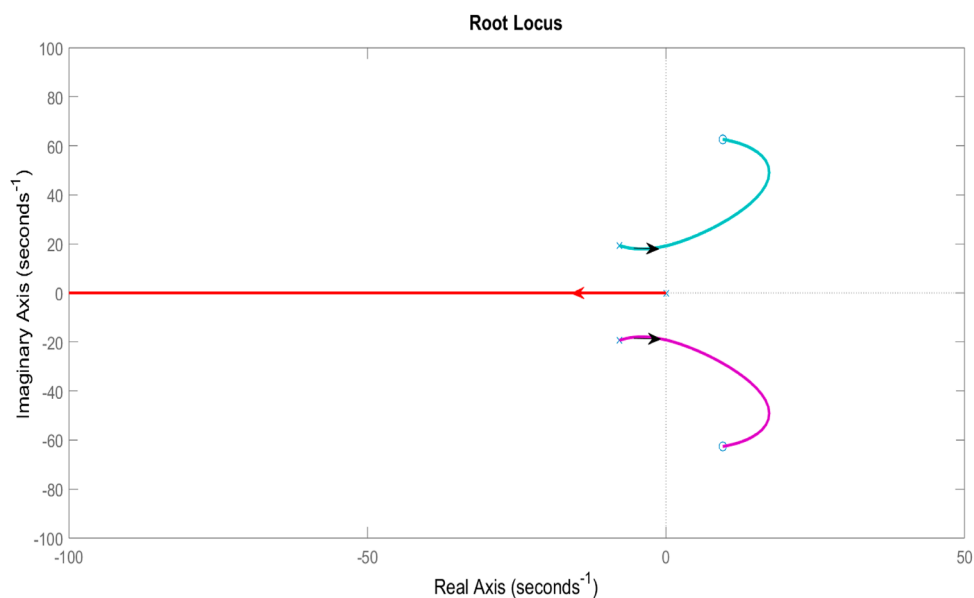
Figure 1. Root locus diagram when yaw velocity is used as feedback.

achieved with the use of yaw velocity feedback because there are also two open loop zeros at s = 0 in Equation (7) which prevent the pole s = 0 from moving away as closed loop poles are attracted to open loop zeros. In the root locus diagram produced using Equation (7) as given in Figure 1 (where arrows indicate the direction of the migration of closed loop poles as the control gain is increased), the pole s = 0 is attracted to one of the zeros s = 0 and is not moved with the increase of the control gain. However, the second zero at s = 0 helps to move the unstable poles to the negative side, and therefore the dynamic instability in independently rotating wheelset can be overcome with passive yaw damping.

On the other hand, the use of relative rotational velocity between the two wheels does not have a similar problem as there is no zero at s = 0 in equation 8. Figure 2 shows the corresponding root locus diagram, where a passive yaw damping is also added for the dynamic stability. As the control gain increases, the closed loop pole at s = 0 is moved from s = 0 towards the negative side, indicating the provision of steering actions. Caution is needed when tuning this control gain, as it also has the opposite effect to the yaw damping for the dynamic instability and this is demonstrated in Figure 2 with the two poles stablised through the use of yaw damping now moving towards the unstable region, so there is clearly a trade-off between the steering and stability.

3. Semi-active control approach

The control of independently rotating wheels through the use of semi-active means has been shown to be possible in computer simulations at IAVSD2023 [12] and is now backed up with the theoretical analysis above. This paper provides a more comprehensive evaluation of the active steering of independently rotating wheelsets using semi-active means

Figure 2. Root locus diagram when relative rotational velocity is used as feedback.

(via the use of magnetorheological or MR dampers). Figure 3(a) shows the overall control schedule for each wheelset. A magnetorheological damper (MR damper) in the yaw direction, or in practice two linear MR dampers placed on either side of each wheelset (as illustrated in Figure 3(b)), is used to provide the controllable yaw torque. As discussed in Section 2, there are two parts of the control law. The stability of wheelset is provided by controlling the yaw velocity of each wheelset as feedback or by controlling the relative yaw velocity between the body and each wheelset by measuring the actuator movement directly. The steering/guidance control is achieved by producing a control effort proportional to the relative rotational speed of the two wheels of each wheelset such that the independently rotating wheelset would behave in a similar way to its solid axle counterpart. The control law for each wheelset is given in equation 9 and the tuning and optimisation of the control gains are carried out in two steps with the use of a root locus diagram to place the eigenvalues in the desired locations as demonstrated in Figures 1 and 2. The stability control gain G_1 is first tuned to give a damping ratio between 20 and 30% to provide a sufficient stability margin for the instability mode. The value obtained for G_1 is then added to the wheelset model and used in the second step to find the guidance control gain G_2, which is set to move the pole from s = 0 to around s = 5 in this study. This would give a time constant of 0.2s for a relatively fast response for steering/guidance control.

The force/torque demand from the wheelset controller is used to vary the damping coefficient of the MR damper as given in Equation (10). The wheelset control is expected not to demand power injection (i.e. negative power), but a condition is added in the MR controller to set the damping coefficient to a minimum anyway. The damping coefficient is then converted to a current input using a lookup table. Additional local feedback control for the MR dampers is also designed to ensure fast and robust responses of the dampers to
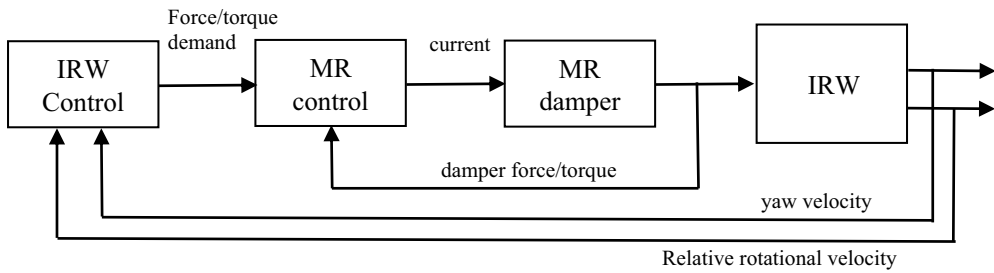
(a) Overall control scheme
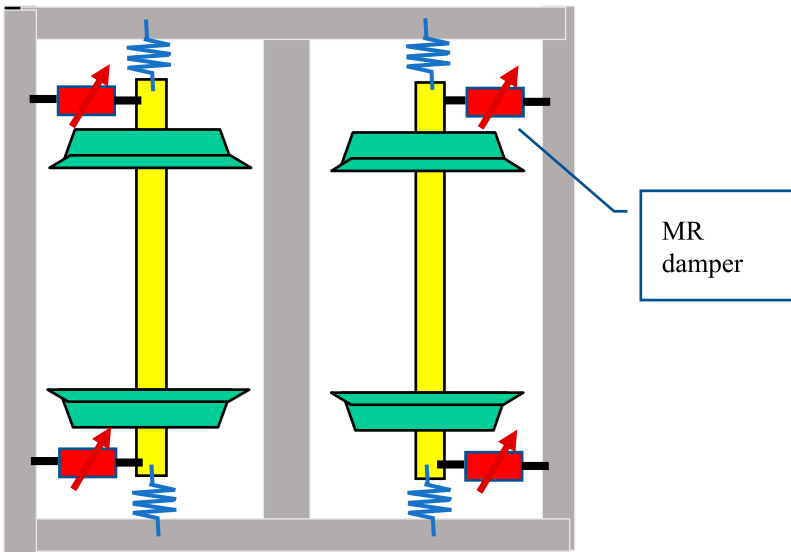
(b) Arrangement of MR dampers

Figure 3. Semi-active control scheme with MR damper.

deliver the control effort as demanded by the wheelset control law.

$$T_X = -G_1 \dot{\psi} + G_2 \Delta\omega \tag{9}$$

$$C_{MR} = \begin{cases} \frac{F_{demand}}{\Delta V}, & \frac{F_{demand}}{\Delta V} \geq 0 \\ C_{min}, & \frac{F_{demand}}{\Delta V} < 0 \end{cases} \tag{10}$$

Two feedback measurements are required for the wheelset control law. The relative rotational speed can be measured by using tachometers/digital encoders on both sides of a wheelset. The yaw rate can be obtained via axle-mounted gyroscope directly. Alternately, the relative displacement of the MP dampers may be measured and the differentiation could be used to produce the relative velocity between the wheelset and the bogie frame which is equally effective for stability as mentioned above.
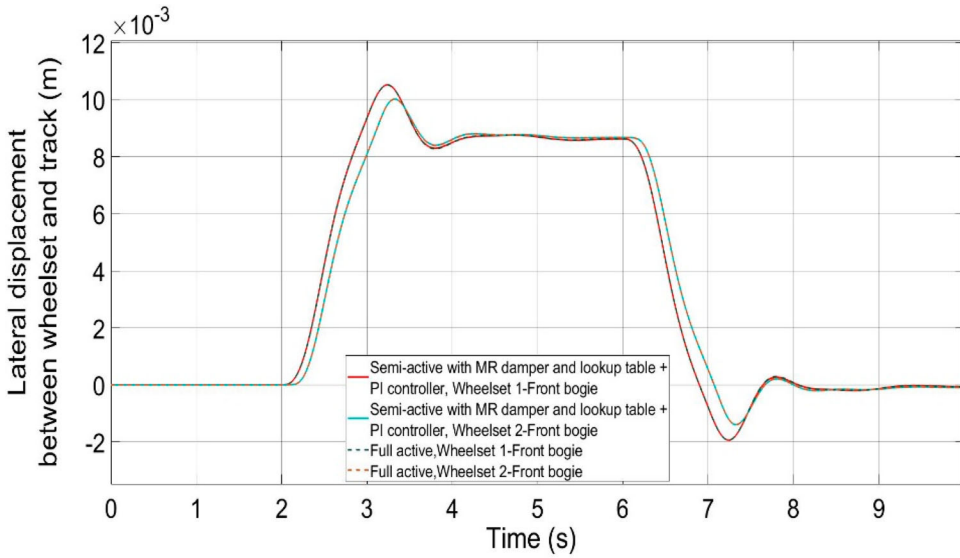
(a) front bogie
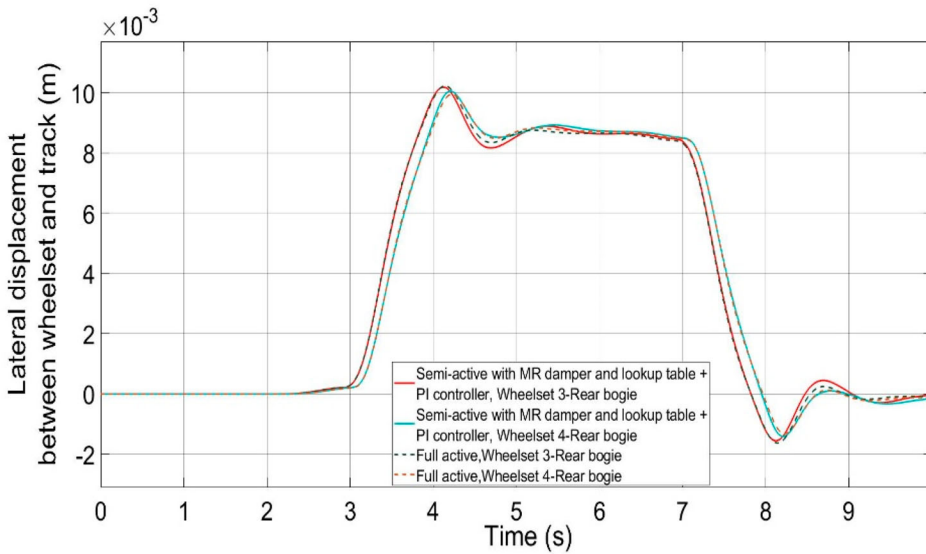
(b) rear bogie

Figure 4. Wheelset lateral deflection (on low-speed curve).

4. Simulation results

Mathematical models for a conventional bogie vehicle are used in computer simulations to evaluate the performance of the proposed control scheme. The model of the MR dampers with the local force controller is also included to account for the effect of potential control
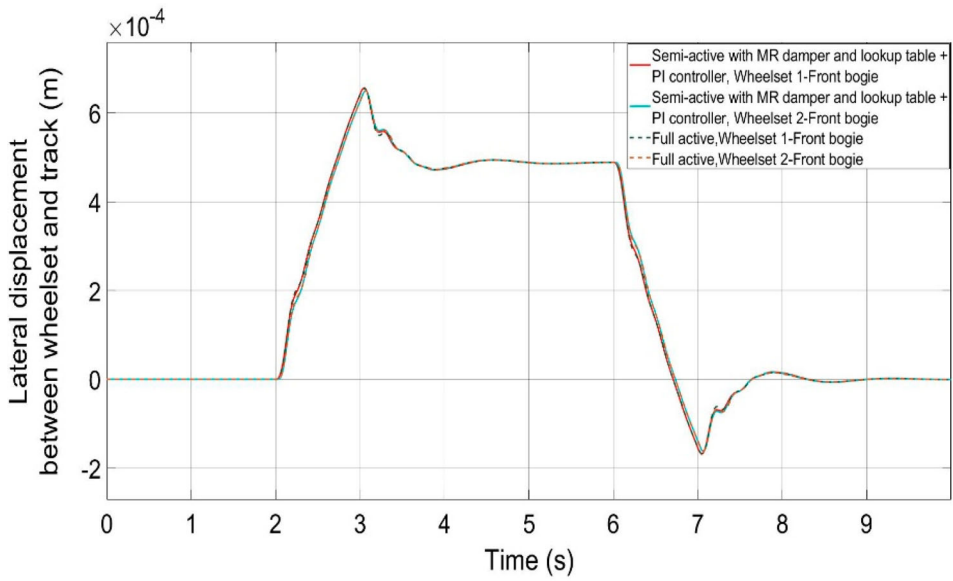
(a) front bogie
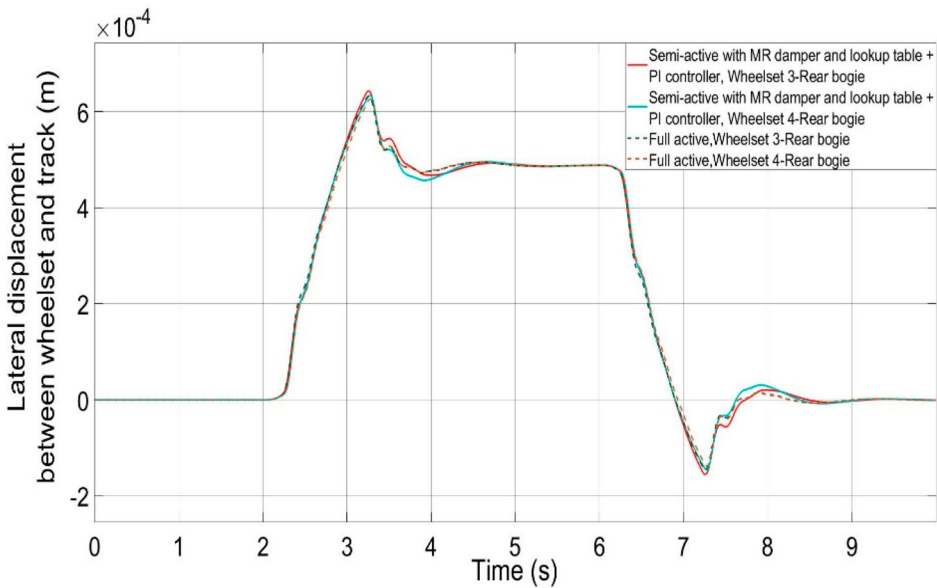
(b) rear bogie

Figure 5. Wheelset lateral deflection (on high-speed curve).

lag. The vehicle model is based on a high-speed intercity vehicle with some modifications to take full advantage of the semi-active control system. The conventional solid axle wheelsets are replaced with independently rotating wheelsets. Also, the longitudinal stiffnesses in the primary suspensions and the secondary yaw damping are removed as the stability is now
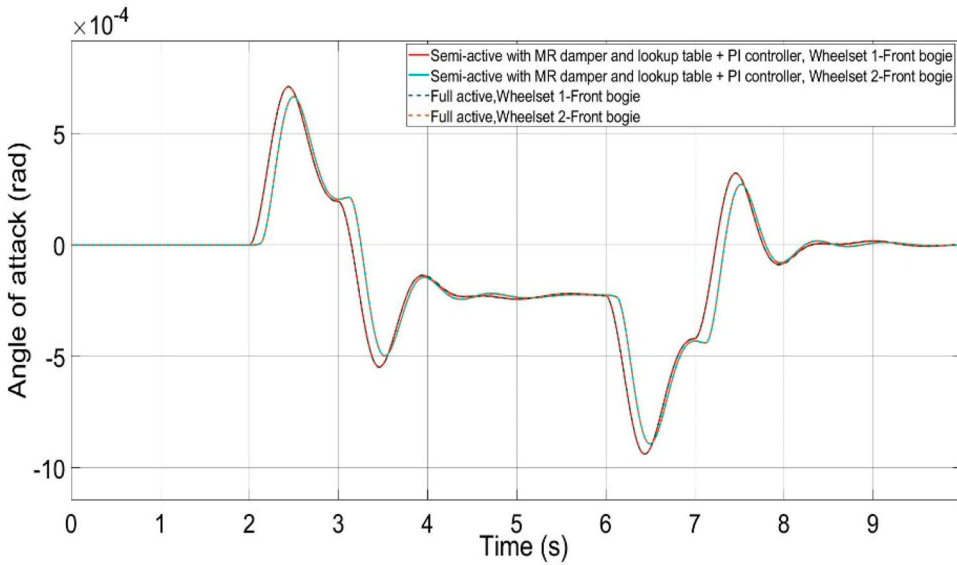
Figure 6. Wheelset angle of attack at the front bogie (on low-speed curve).
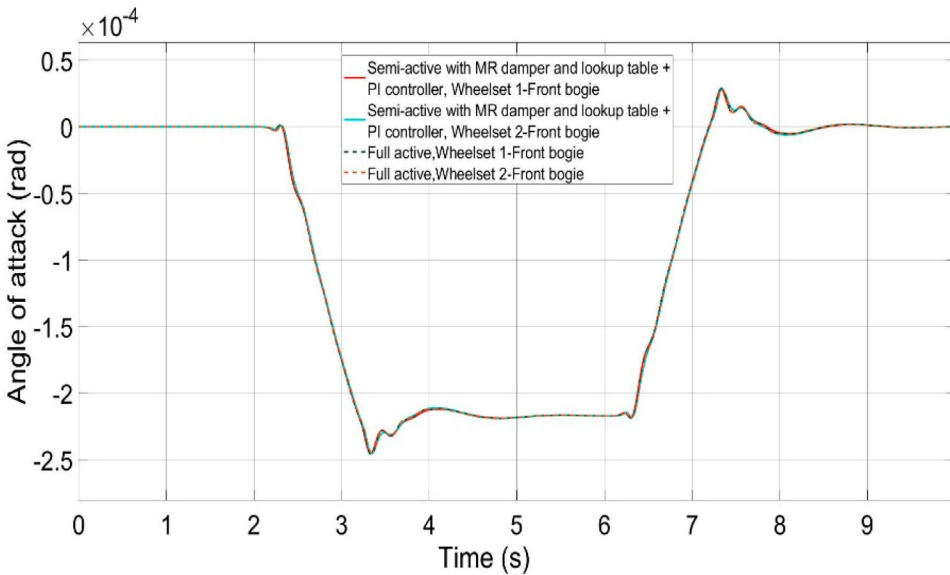
Figure 7. Wheelset angle of attack at the front bogie (on high-speed curve).

provided by the proposed control system. Values of some key parameters of the models can be found in the list of symbols and parameters. For comparison, a full active control scheme is also used in the computer simulation. The full active control applies the same control laws as defined in Equation (9), but ideal actuation is assumed which represents the best scenario of the full active control. The following scenarios are examined as listed below. There is a cant deficiency of 6° on both low and high-speed curves. The measured track irregularities are real mis-alignment of a UK intercity mainline, whereas the generically
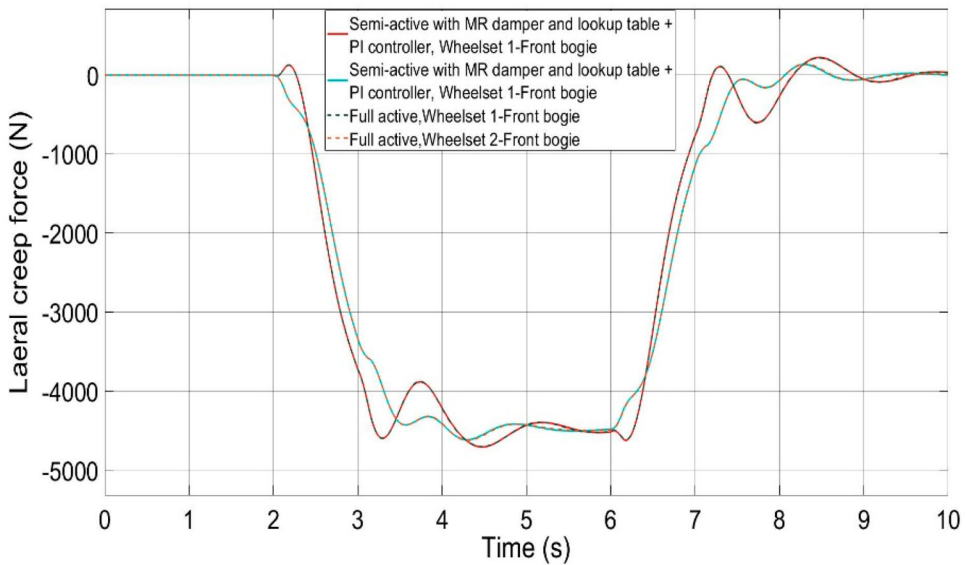
Figure 8. Wheelset lateral creep force at the front bogie (on low-speed curve).

generated irregularities represent a broader spectrum of random data and provide a more severe testing condition for the evaluation.

(1) Low-speed curve at 72 km/h (20 m/s), with a curve radius of 200 m and cant angle of 6°
(2) High-speed curve at 300 km/h (83 m/s), with a curve radius of 3500 m and cant angle of 6°
(3) Straight track with measured track irregularities
(4) Straight track with generically generated irregularities

Figure 4(a, b) shows the wheelset lateral deflections at the front and rear bogies on the low-speed curve respectively, and Figure 5(a, b) is those on the high-speed curve. On the constant curves, the lateral deflections of all wheelsets are the same and almost identical to those of full active control, indicating an ideal curving condition.

The wheelsets also form the same angle of attack on both low and high-speed curves in the same way as the full active control as shown in Figures 6 and 7. This provides an equal amount of lateral creep forces, which share evenly between all the wheelsets the vehicle centrifugal force due to the cant-deficiency as confirmed in Figures 8 and 9. The control effort on curves is low as shown in Figures 10 and 11. This is because the longitudinal creep forces of independently rotating wheelset are in general very small due to the free rotation between the two wheels.

On a straight track, Figures 12 and 13 show that the wheelsets follow the track irregularities well, and there is no tendency to drift from the central line which would mean wheelsets running on flanges in practice. For the measured track irregularities, the maximum wheel-rail deflections are under 5 mm, well within the flange contact. On the generic generated irregularities, the peak lateral deflections appear to exceed 10 mm. However, this
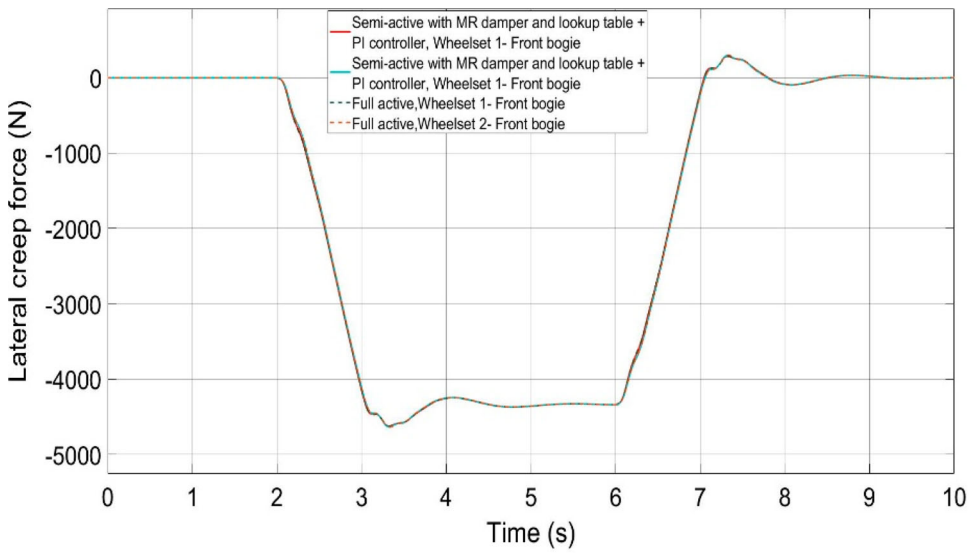
Figure 9. Wheelset lateral creep force at the front bogie (on high-speed curve).
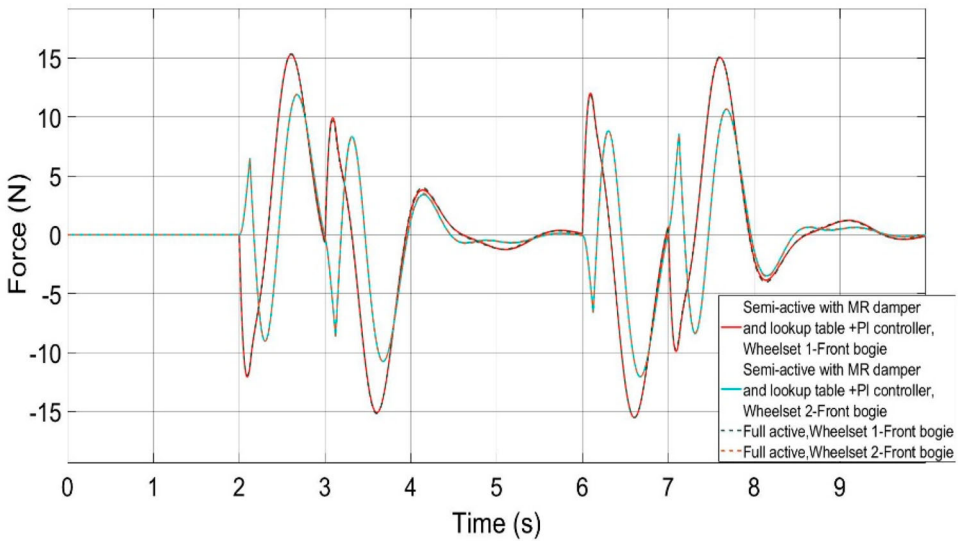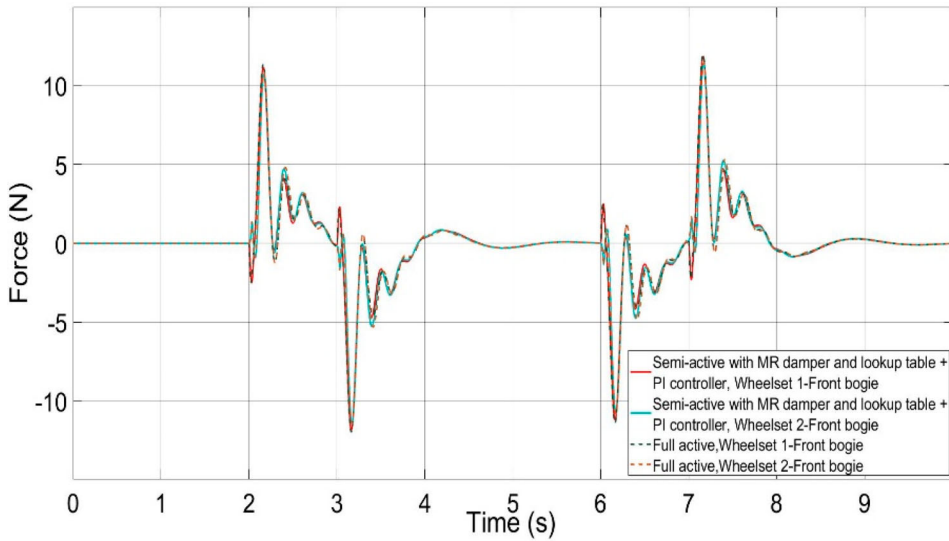

Figure 10. Control effort at the front bogie (on low-speed curve).

is mainly due to the use of a constant conicity in the simulation models and is not expected to occur with the non linear wheelset profiles as the equivalent conicity would substantially increase closer to the wheel flanges which would reduce the lateral deflections.

In general, the control effort required for independently rotating wheelsets is much higher to overcome the track irregularities than that needed to negotiate curves as the much faster control actions are necessary to respond to the components of high frequencies in the track mis-alignment, as illustrated in Figures 14 and 15 in comparison to Figures 8 and

**Figure 11.** Control effort at the front bogie (on low-speed curve).
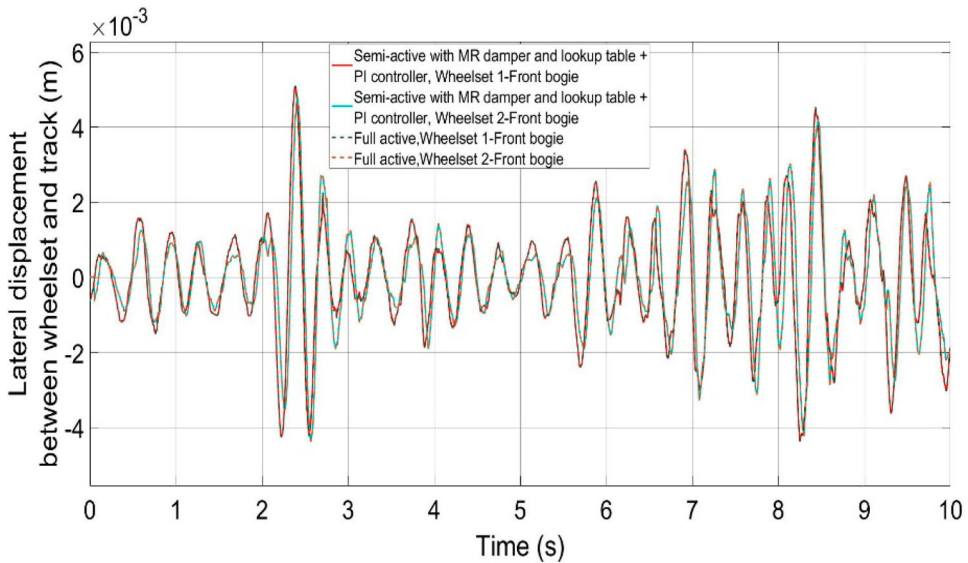
Figure 12. Wheelset-rail deflection with measured track irregularities (V = 50 m/s).

9. The size and power requirement of the control devices are therefore determined by the severity of the track irregularities and vehicle operation speed.
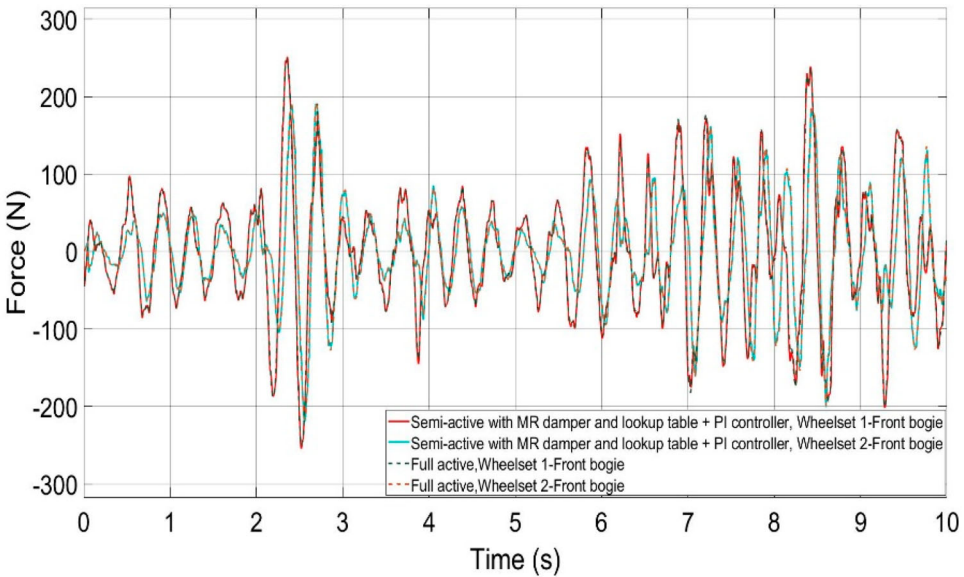
5. Conclusions

This paper has presented a comprehensive study of the semi-active strategies for the steering and stability control of railway vehicles with independently rotating wheelsets, with detailed theoretical analysis and computer simulation evaluation.
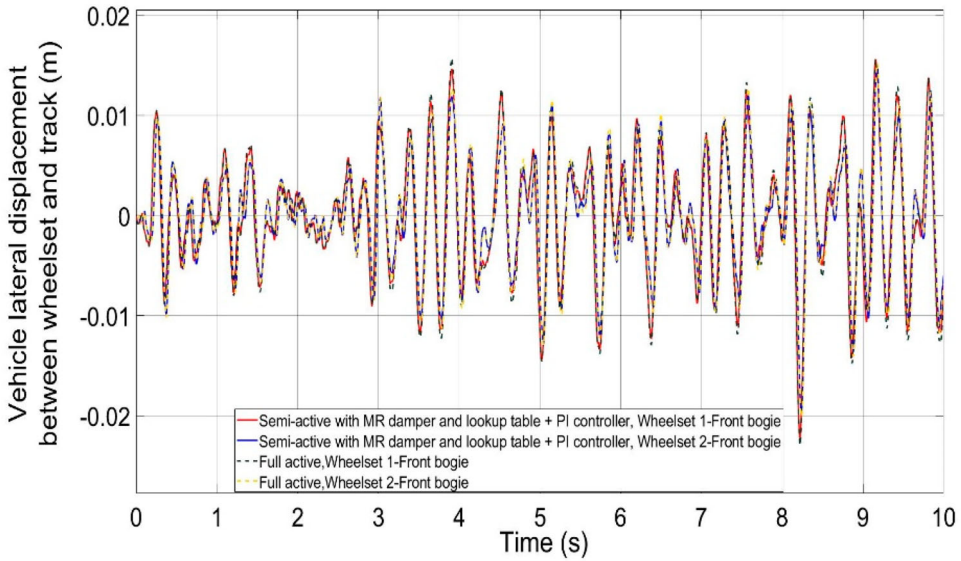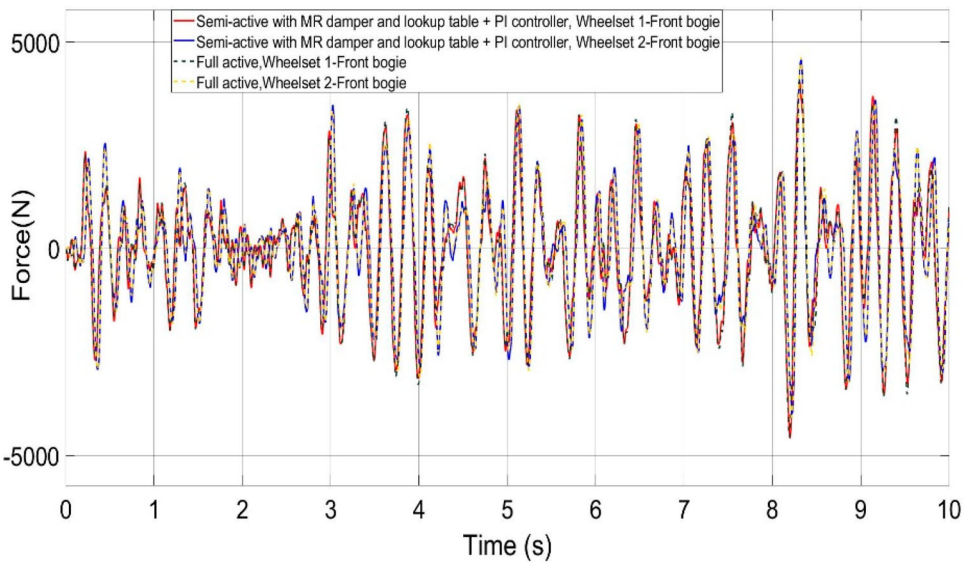
Figure 13. Wheelset-rail deflection with generic track irregularities (V = 83 m/s).

Figure 14. Control effort with measured track irregularities (V = 50 m/s).

The study has demonstrated that the control of independently rotating wheelset for guidance and stability can be achieved without the use of the more costly full active control and it is possible to formulate control strategies such that no power injection in the control is necessary. The semi-active control scheme with controllable MR dampers used in this study has been shown to perform as well as full active control on all four different track input scenarios. Ideal curving conditions are achieved on the curved track inputs with the

Figure 15. Control effort with generic track irregularities (V = 83 m/s).

lateral deflections and angles of attack of all the wheelsets being identical. The wheelsets also follow the track well on straight track inputs with no drifting away from the central line to the flange contact. The control effort is relatively small in comparison to the control of solid-axle wheelsets and the size and power requirement of the control devices are mainly determined by the vehicle operation speed and severity of track irregularities.

Acknowledgements

Disclosure statement

No potential conflict of interest was reported by the authors.

References

[1] Bruni S, Goodall RM, Mei TX, et al. Control and monitoring for railway vehicle dynamics. Veh Syst Dyn. 2007;45(7/8):743–779. doi:10.1080/00423110701426690
[2] Fu B, Giossi R L, Persson R, et al. Active suspension in railway vehicles: a literature survey. Railw Eng Sci. 2020;28:3–35. doi:10.1007/s40534-020-00207-w
[3] Mei TX, Goodall RM. Robust control for independently-rotating wheelsets on a railway vehicle using practical sensors. IEEE Trans Control Syst Technol. July, 2001;9(4):599–607. ISSN 1063-6536.
[4] Mei TX, Goodall RM. Practical strategies for controlling railway wheelsets with independently rotating wheels. ASME J Dyn Syst Meas Control. 2003;125/3:354–360.
[5] Perez J, Mauer L, Busturia JM. Design of active steering systems for bogie-based railway vehicles with independently rotating wheels. Veh Syst Dyn. 2002;37(sup1):209–220. doi:10.1080/00423114.2002.11666233

[6] Mei TX, Qu KW, Li H. Control of wheel motors for the provision of traction and steering of railway vehicles. IET Power Electron. 2014;7(9):2279–2287. doi:10.1049/iet-pel.2013.0882

[7] Heckmann A, Daniel L, Grether G, et al. From scaled experiments of mechatronic guidance to multibody simulations of DLR's next generation train set. Proceedings of the 25th international symposium on dynamics of vehicle on roads and tracks; 14-18 August 2017; Rockhampton, Queensland.

[8] Liang B, Iwnicki SD. Independently rotating wheels with induction motors for high-speed trains. J Control Sci Eng. 2011;2011: 1–7. doi:10.1155/2011/968286

[9] Wickens AH. Dynamic stability of articulated and steered railway vehicles guided by lateral displacement feedback. Veh Syst Dyn. 1994;23(sup1):541–553. doi:10.1080/00423119308969539

[10] Michitsuji Y, Suda Y. Running performance of power steering railway bogie with independently rotating wheels. VehSyst Dyn. 2006;44(sup1):71–82.

[11] Baiasu D, Ghita G, Sebesan I. Control system with magnetorheological fluid device for mitigation of the railway vehicle oscillations. 13th ERME2012; July 2012; Ankara.

[12] Mei TX, Zaeim A, Li H. Control of independently rotating wheels with MR dampers. IAVSD2023; 20-25 August, 2023; Ottawa.